DOCKETED

Docket Number:	09-AFC-07C
Project Title:	Palen Solar Power Project - Compliance
TN #:	203011
Document Title:	Methodology to Assess Potential Glint and Glare Hazards from Concentrating Solar Power Plants (2011) Clifford, et al
Description:	Article
Filer:	Janet Schultz
Organization:	California Energy Commission
Submitter Role:	Commission Staff
Submission Date:	8/29/2014 1:08:51 PM
Docketed Date:	8/29/2014

Methodology to Assess Potential Glint and Glare Hazards From Concentrating Solar Power Plants: Analytical Models and Experimental Validation

Clifford K. Ho
e-mail: ckho@sandia.gov

Cheryl M. Ghanbari

Richard B. Diver

Concentrating Solar Technologies Department,
Sandia National Laboratories,
P.O. Box 5800,
Albuquerque, NM 87185-1127

With a growing number of concentrating solar power systems being designed and developed, the potential impact of glint and glare from concentrating solar collectors and receivers is receiving increased attention as a potential hazard or as a distraction for motorists, pilots, and pedestrians. This paper provides analytical methods to evaluate the irradiance originating from specularly and diffusely reflecting sources as a function of distance and characteristics of the source. Sample problems are provided for both specular and diffuse sources, and validation of the models is performed via testing. In addition, a summary of safety metrics is compiled from the literature to evaluate the potential hazards of calculated irradiances from glint and glare for short-term exposures. Previous safety metrics have focused on prevention of permanent eye damage (e.g., retinal burn). New metrics used in this paper account for temporary after-image, which can occur at irradiance values several orders of magnitude lower than the irradiance values required for irreversible eye damage. [DOI: 10.1115/1.4004349]

1 Introduction

Assessment of the potential hazards of glint and glare from concentrating solar power plants is an important requirement to ensure public safety [1–3]. Glint is defined as a momentary flash of light, while glare is defined as a more continuous source of excessive brightness relative to the ambient lighting. Hazards from glint and glare from concentrating solar power plants include the potential for permanent eye injury (e.g., retinal burn) and temporary disability or distractions (e.g., after-image), which may impact people working nearby, pilots flying overhead, or motorists driving alongside the site.

Applications and certifications for solar thermal power plants require an assessment of "visual resources" at the site (e.g., Refs. [4–8]), but rigorous and uniform treatment of glint and glare are lacking. Several previous studies [1–3] investigated the impact of specular reflections using permanent eye damage as a metric. The purpose of this paper is to provide a general assessment method that can be used to evaluate potential hazards of glint and glare for all of the primary concentrating solar power technologies: (1) power-tower systems, (2) linear concentrator systems (e.g., parabolic troughs, linear Fresnel), and (3) dish/engine systems. In particular, this paper provides analytical solutions to evaluate the irradiance originating from both specularly and diffusely reflecting sources as a function of distance and characteristics of the source. In addition, tests were conducted at the National Solar Thermal Test Facility (NSTTF) at Sandia National Laboratories to validate the models. Modeling results (analytical and ray-tracing) were compared to the data, which showed an excellent agreement. The measured and/or calculated irradiances can be compared against the compiled safety metrics to determine safe perimeter zones or regions where personal protective equipment may be needed for short-duration exposures.

2 Review of Ocular Safety Metrics

This section summarizes the ocular safety metrics introduced by Ho et al. [9] for short-term exposures of bright light. Two variables are required for the ocular impact assessment: the retinal irradiance and the subtended angle (size) of the glare source. The retinal irradiance can be calculated from the total power entering the pupil and the retinal image area. The diameter, d_r, of the image projected onto the retina (assuming circular images) can be determined from the subtended source angle (ω), which can be calculated from the source size (d_s), radial distance (r) between the eye and the source, and the focal length of the eye ($f \cong 0.017$ m [3]), as follows (see Fig. 1):

$$d_r = f\omega \quad \text{where } \omega = d_s/r \tag{1}$$

If the irradiance at a plane in front of the cornea, E_c (W/m^2), is known, the power entering the pupil can be calculated as the product of the corneal irradiance and the pupil area (the daylight adjusted pupil diameter, d_p, is ~2 mm). The power is then divided by the retinal image area and multiplied by a transmission coefficient, $\tau(\sim 0.5)$ [10], for the ocular media (to account for absorption of radiation within the eye before it reaches the retina) to yield the following expression for the retinal irradiance:

$$E_r = E_c \left(\frac{d_p^2}{d_r^2} \right) \tau \tag{2}$$

It should be noted that Brumleve [1] includes an additional coefficient (ν) to account for the fraction of solar irradiance between 400 and 1400 nm, but this has been included in the transmission coefficient, τ, above. As an example, the retinal irradiance caused by viewing the sun directly can be calculated using Eqs. (1) and (2) with $E_c = 0.1$ W/cm^2, $d_p = 0.002$ m, $f = 0.017$ m, $\omega = 0.0094$ rad, and $\tau = 0.5$, which yields a retinal irradiance, E_r, of ~8 W/cm^2. The ocular parameters are taken from Refs. [1] and [3]. Note that

Contributed by the Solar Energy Division of ASME for publication in the JOURNAL OF SOLAR ENERGY ENGINEERING. Manuscript received November 3, 2010; final manuscript received May 25, 2011; published online August 5, 2011. Assoc. Editor: Manuel Romero Alvarez.

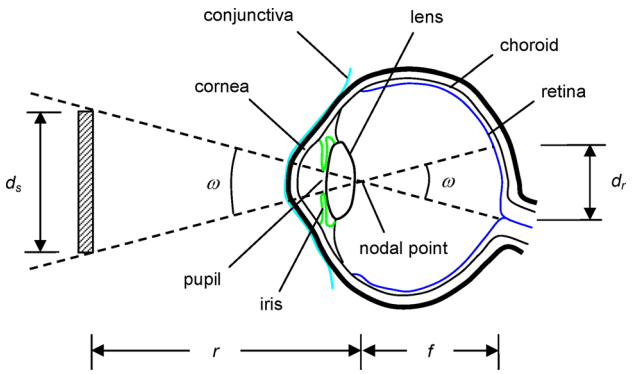

Fig. 1 Image projected onto the retina of the eye

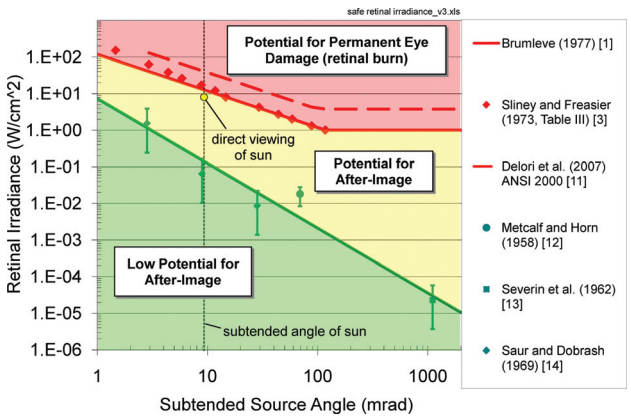

Fig. 2 Potential impacts of retinal irradiance as a function of subtended source angle. Data for irreversible eye damage are from Refs. [1,10,11] for 0.15 s exposure (typical blink response time). Data for temporary after-image are from Refs. [12–14].

the retinal irradiance is significantly higher than the irradiance at the entrance of the eye. The calculated irradiances and thresholds used to determine ocular impacts assume a standard solar spectral distribution (ASTM G173-03), where the majority of the energy and short-duration exposure impacts are due to radiation within the visible spectrum (~380 to 800 nm). Longer-term exposures (e.g., for worker safety) may be additionally concerned with radiation in the ultraviolet and infrared spectra.

Figure 2 summarizes the potential impact of different retinal irradiances as a function of subtended source angle for short-term exposures. Three regions are shown: (1) potential for permanent eye damage (retinal burn), (2) potential for temporary after-image (flash blindness), and (3) low potential for temporary after-image. If the retinal irradiance is sufficiently large for a given subtended source angle, permanent eye damage from retinal burn may occur [3,10,11]. Note that as the subtended source angle increases, the safe retinal irradiance threshold decreases. For a given retinal irradiance, a larger subtended source angle yields a larger retinal image area and delivers a greater power to the retina that cannot be as easily dissipated from the perimeter of the "hot" retinal image as with a smaller image area. Brumleve provides a lower threshold for the retinal irradiance corresponding to permanent eye damage using data from Ref. [3]

$$E_{r,\text{burn}} = 0.118/\omega \quad \text{for } \omega < 0.118 \text{ rad} \tag{3}$$

$$E_{r,\text{burn}} = 1 \quad \text{for } \omega \geq 0.118 \text{ rad} \tag{4}$$

where $E_{r,\text{burn}}$ is the retinal burn threshold (W/cm^2) and ω is the subtended angle (rad). Below the retinal burn threshold, a region exists where a sufficiently high retinal irradiance may cause temporary after-image or flash blindness, which is caused by bleaching (oversaturation) of the retinal visual pigments [3]. When this occurs, a temporary after-image appears in the visual field (e.g., the effect after viewing a camera flash in a dim room). The size and impact of the after-image in the field of view depend on the size of the subtended source angle. For a given retinal irradiance, smaller source angles yield smaller after-images, and the potential impact is less. In Fig. 2, data from Refs. [12–14] were used to fit a lower threshold for potential after-image effects. In Refs. [12–14], people were subjected to different source luminances, and their recovery time was recorded. The minimal retinal irradiance based on the illuminance[1] and subtended source angle that yielded at least 1 s of after-image is shown in Fig. 2. Error bars represent uncertainty in the pupil diameter (2–8 mm) [13,14] and variability in subject response [12]. A fit corresponding to these data that yielded the minimal retinal irradiances that caused an after-image is as follows:

$$E_{r,\text{flash}} = \frac{3.59 \times 10^{-5}}{\omega^{1.77}} \tag{5}$$

where $E_{r,\text{flash}}$ is the threshold for potential after-image (W/cm^2) and ω is the subtended source angle (rad). Values of retinal irradiance below $E_{r,\text{flash}}$ have a low potential for after-image impact. Note that, as plotted in Fig. 2, a brief direct viewing of the sun (0.15 s) has a high potential for producing after-image effects.

3 Modeling Approach

This section presents analytical methods for calculating irradiance caused by specular and diffuse reflections of sunlight as a function of distance and other characteristics of the source. Specular reflections occur from polished mirror-like surfaces so that the reflected angle is equal to the incident angle relative to the surface normal. Diffuse reflections occur from uneven or rough surfaces that scatter the incident radiation such that the radiance is approximately uniform in all directions (see Fig. 3). The following sections provide methods to calculate the irradiance from specular and diffuse reflections. Once the irradiance is determined, the equations in the previous section can be used to calculate the retinal irradiance for comparison against the safe retinal irradiance metrics presented in Fig. 2.

3.1 Analytical Model of Specular Reflections. Direct specular solar reflection from mirrors can cause glint and glare hazards when heliostats are in standby positions (reflecting the sun at locations other than the receiver). Specular solar reflections from dishes and parabolic troughs can cause glint and glare hazards when the collectors are in off-axis positions (e.g., when moving from a stowed position to a tracking position). For parabolic troughs, glint and glare from specular reflections can also occur when the sun is low in the horizon and aligned with the axis of the trough, causing reflected rays to spill from the end of the trough.

3.1.1 Point-Focus Collectors. An analytical model of beam irradiance resulting from specular solar reflections from a

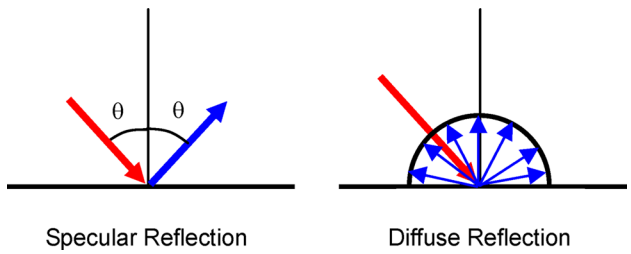

Fig. 3 Illustration of specular versus diffuse reflections

[1]The ratio of spectrally weighted solar illuminance to solar irradiance at the earth's surface yields a conversion factor of ~100 lumens/W.

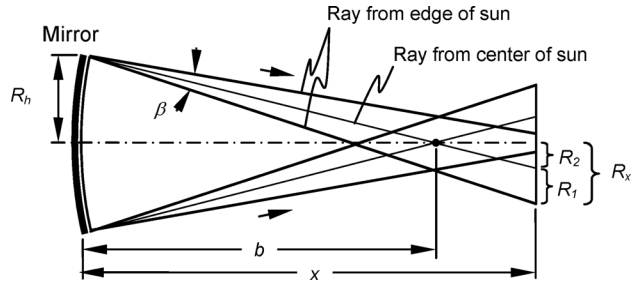

Fig. 4 Geometry of specular solar reflections from a focused mirror where *b* is the focal length, R_h is the radius of the mirror, β is the beam divergence angle, and R_x is the radius of the beam cross section at distance, *x*, from the mirror (adapted from Ref. [1])

point-focus mirror has been derived [1] with the following assumptions (see Fig. 4):

- uniform sun radiant intensity (no limb darkening)
- round, focused, continuous surface mirrors
- no cosine losses, off-axis aberrations, or atmospheric attenuation
- uniform irradiance in beam cross section.

The assumptions above will generally produce the largest beam irradiance, but the assumption of uniform sun radiant intensity averages the irradiance over the entire beam. Using a nonuniform solar intensity creates larger peak irradiances toward the center of the beam. Comparisons with a ray-tracing model (ASAP®) show that the difference in peak irradiance is about 25–30% at the focal length, but the difference can be greater at other distances.

The beam irradiance, E_{beam} (W/cm^2), is then calculated as the product of the direct normal irradiance, E_{DNI} (W/cm^2), the mirror reflectivity, ρ, and the area concentration ratio, C

$$E_{\text{beam}} = \rho E_{\text{DNI}} C \tag{6}$$

The direct normal irradiance, E_{DNI}, at the earth's surface is approximately 0.1 W/cm^2. The area concentration ratio, C, can be calculated as follows assuming a circular mirror area, A_h, with radius, R_h, and a circular beam area, A_x, with radius, R_x, at a distance, x, from the mirror,

$$C = \frac{A_h}{A_x} = \left(\frac{R_h}{R_x}\right)^2 \tag{7}$$

The radius, R_x, of the beam is comprised of two components,

$$R_x = R_1 + R_2 \tag{8}$$

where R_1 is caused by beam spreading due to the subtended angle of the sun and mirror contour inaccuracies (slope error), and R_2 represents the focusing and defocusing characteristics of the beam at a distance that is less than or greater than the focal length. The beam divergence, R_1, at a distance, x, from the mirror is defined by the sun half-angle ($\sim$4.7 mrad) and any additional slope errors caused by mirror inaccuracies,

$$R_1 \approx x \tan\left(\frac{\beta}{2}\right) \tag{9}$$

where $\beta/2$ is the half-angle (rad) of the total beam divergence. According to Ref. [1], this approximation has an error that is less than 0.3% for $b/R_h > 18$. R_2 can be defined using similar triangles as shown in Fig. 4, where b is the focal length,

$$\frac{R_2}{|x-b|} = \frac{R_h}{b} \Rightarrow R_2 = \left|\frac{x}{b} - 1\right| R_h \tag{10}$$

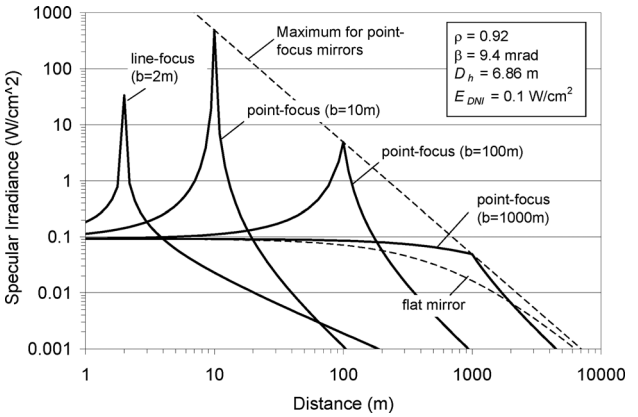

Fig. 5 Specular irradiance at the cornea as a function of distance from point-focus and line-focus mirrors with different focal lengths, *b*, for a solar irradiance of 0.1 W/cm^2

Using Eqs. (7)–(10) in Eq. (6), and the approximation that $\tan(\beta/2) = \beta/2$ when $\beta/2$ is small, yields the following expression for the beam irradiance (W/cm^2):

$$E_{\text{beam}} = \rho E_{\text{DNI}} \left(\frac{x\beta}{D_h} + \left|\frac{x}{b} - 1\right|\right)^{-2} \text{(point-focus collectors)} \tag{11}$$

where $D_h = 2\,R_h$. The beam irradiance can also be presented in units of "suns" by dividing Eq. (11) by E_{DNI} ($\sim$0.1 W/cm^2). The maximum beam irradiance occurs at the focal length, $x = b$. In addition, the beam irradiance from a flat mirror can be calculated by setting $b = \infty$ in Eq. (11). The specular beam irradiance for several focal lengths is plotted in Fig. 5 as a function of distance, x, from the mirror. The reflectivity, ρ, is assumed to be 0.92, and the total beam divergence angle, β, is assumed to be equal to 9.4 mrad. The effective diameter of the mirror, D_h, is calculated from the total reflective surface (37 m^2) of each heliostat used at the National Solar Thermal Test Facility at Sandia National Laboratories in Albuquerque, NM,

$$D_h = \left(\frac{4A_h}{\pi}\right)^{0.5} \tag{12}$$

In addition to the beam irradiance, we also need to determine the size of the reflected sun image observed in the mirror to determine the subtended source angle and the retinal irradiance to assess potential ocular hazards in Fig. 2. It should be noted that the size of the reflected sun image in the mirror as viewed by an observer is different than the projected beam size calculated in Eqs. (8)–(10). An observer located within the projected beam and away from the focal point of a mirror may see a reflected image of the sun that occupies only a very small portion of the mirror. At the focal point, an observer would see a reflected image of the sun that fills the mirror.

As defined in Eq. (6), the beam irradiance is proportional to the concentration ratio, which is equal to the area ratio of the mirror and the beam size. It follows that the relative spot size of the reflected image of the sun in the mirror observed at a given distance, x, is proportional to the measured irradiance at that location. Then, once the beam irradiance, E_{beam}, is determined for the focused mirror using Eq. (11), the spot size of the reflected image of the sun observed in the focused mirror can be estimated relative to the equivalent spot size observed on an infinitely large flat mirror ($b \to \infty$, $D_h \to \infty$) at the same location,

$$\frac{A_{\text{spot}}}{A_{\text{spot,flat}}} = \left(\frac{d_{\text{spot}}}{d_{\text{spot,flat}}}\right)^2 = \left(\frac{x\omega_{\text{spot}}}{x\beta}\right)^2 = C = \frac{E_{\text{beam}}}{\rho E_{\text{DNI}}}$$

$$\Rightarrow \omega_{\text{spot}} = \beta\sqrt{\frac{E_{\text{beam}}}{\rho E_{\text{DNI}}}} \tag{13}$$

where A_{spot} is the area of the reflected spot image on a mirror as viewed by an observer a distance, x, away from the mirror, the subscript "flat" denotes a flat mirror that is sufficiently large so that the entire reflected image of the sun can be seen by the observer, d_{spot} is the diameter of the reflected image on the mirror, ω_{spot} is the subtended angle of the reflected sun image on the mirror as observed from a prescribed distance, and β is the beam divergence angle caused by the sun angle and slope error. For an infinitely large flat mirror, the diameter of the reflected sun image observed a distance, x, away from the flat mirror is approximately $x\beta$, and, according to Eq. (11), the beam irradiance is ρE_{DNI} as $b\rightarrow\infty$ and $D_h\rightarrow\infty$. Thus, if the measured irradiance, E_{beam}, is greater (or less) than ρE_{DNI}, the observed size and subtended angle, ω_{spot}, of the reflected spot image of the sun on the focused mirror will be greater (or less) than the size and subtended angle, β, of the reflected sun image on a large flat mirror at the same location. Equation (13) can be intuitively checked at two distances, $x\approx 0$ and $x=b$. At $x\approx 0$ (observer located immediately next to the mirror), Eq. (11) yields a beam irradiance, E_{beam}, equal to ρE_{DNI}, and Eq. (13) yields a subtended spot angle equal to β, which is expected at $x\approx 0$ (the mirror essentially appears flat to the observer, and the subtended angle of the reflected sun image is the same as looking at a reflection in a flat mirror). At $x=b$, Eqs. (11) and (13) yield a subtended angle, ω_{spot}, of the reflected sun image equal to D_h/b, which indicates that the reflected sun image will fill the entire collector when the observer is at the focal point, as expected.

Using Eq. (13) in Eqs. (1) and (2) yields the following expression for the retinal irradiance, where the corneal irradiance, E_c, is set equal to the beam irradiance, E_{beam}, used in Eqs. (11) and (13),

$$E_r = \frac{\rho E_{\text{DNI}} d_p^2 \tau}{f^2\beta^2} \tag{14}$$

Note that the retinal irradiance in Eq. (14) does not depend on distance from the source (neglecting atmospheric attenuation). As distance increases, both the power entering the pupil and the retinal image area (which is proportional to the square of the subtended source angle) decrease at the same rate. Therefore, the retinal irradiance, which is equal to the power entering the pupil divided by the retinal image area, is independent of distance. The corneal irradiance, however, changes as a function of distance as given by Eq. (11).

The plots in Fig. 5 represent corneal irradiance values (at front of the eye) that could be experienced at different distances and for mirrors of different focal lengths but with prescribed reflectivity, beam divergence angle, and effective mirror size. Equations (11) and (12) can be used to determine the beam irradiance [E_{beam}, which is equivalent to E_c in Eq. (2)] for other mirror characteristics, and then Eqs. (1) and (2) can be used to determine the equivalent retinal irradiance for comparison against the safe retinal irradiance metrics in Fig. 2. For example, at a distance of 200 m, the irradiance from a mirror with a focal length of 100 m and with the prescribed optical characteristics is approximately 0.057 W/cm^2 according to Fig. 5 and Eq. (11). To convert this "corneal irradiance" to a retinal irradiance, Eqs. (1) and (2) are used where the subtended angle, ω, is taken from the subtended angle, ω_{spot}, calculated in Eq. (13) to be 7.4 mrad for $\rho=0.92$, $E_{\text{DNI}}=0.1$ W/cm^2, and $\beta=9.4$ mrad. The retinal irradiance is then found to be 7.2 W/cm^2 with $d_p=0.002$ m, $f=0.017$ m, and $\tau=0.5$ [Eq. (14) yields the same value]. According to Fig. 2, at a subtended source angle of 7.4 mrad, the calculated retinal irradiance of 7.2 W/cm^2 will not produce permanent eye damage. However, the calculated irradiance is sufficient to potentially cause a temporary after-image if one has to view directly at the source. The minimum distance to yield a low potential for after-image in this example is calculated to be $\sim$910 m using Eqs. (5), (11), and (13).

3.1.2 Line-Focus Collectors. The equations derived in Sec. 3.1.1 for determining the specular beam irradiance from point-focus collectors can be readily extended to line-focus (parabolic trough, linear Fresnel) collectors. The primary difference is that the concentration ratio in Eq. (7) is changed since the convergence/divergence of rays caused by the shape of the line-focus mirror is primarily in one dimension (rather than two),

$$C = \frac{A_h}{A_x} = \frac{R_h}{R_x} \tag{15}$$

The resulting irradiance from specular reflections from a line-focus collector then becomes

$$E_{\text{beam}} = \rho E_{\text{DNI}}\left(\frac{x\beta}{D_h} + \left|\frac{x}{b} - 1\right|\right)^{-1} \text{(line-focus collectors)} \tag{16}$$

Equation (16) is similar in form to Eq. (11) for point-focus collectors. However, the irradiance from line-focus collectors decreases less rapidly with the distance past the focal point. Figure 5 shows the specular irradiance from a line-focus collector as a function of distance with an assumed focal length of 2 m, an aperture of 6.86 m, and characteristics as shown in the plot.

The equation that was used to calculate the spot size of the reflected image for point-focus mirrors [Eq. (13)] can be used to describe an *effective* spot size of the reflected sun image in the line-focus mirror.[2] Then, using Eqs. (13) and (16) in Eqs. (1) and (2) yields the same expression for the retinal irradiance as Eq. (14) for point-focus collectors. The retinal irradiance is independent of distance (assuming no atmospheric attenuation) because the retinal image area decreases at the same rate as the irradiance (albeit at a slower rate for line-focus mirrors than for point-focus mirrors); therefore, the retinal irradiance (power entering the eye divided by the retinal image area) is constant.

For the characteristics of a line-focus (trough) collector shown in Fig. 5, the specular irradiance at a distance of 100 m is 1.87×10^{-3} W/cm^2 [Eq. (16)]. The corresponding subtended source angle is 1.34 mrad [Eq. (13)] and the retinal irradiance is 7.2 W/cm^2 [Eq. (14)]. According to Fig. 2 and Eq. (5), this retinal irradiance and subtended source angle will not yield permanent eye damage, but there is a potential for after-image effects if one were to view the specular reflection directly. For this example, the minimum distance to yield a low potential for after-image effects is $\sim$170 m using Eqs. (5), (13), and (16).

3.2 Analytical Model of Diffuse Reflections. In many cases, reflections from receivers, which are used to absorb the concentrated solar irradiance from heliostat, dish, and trough collector systems, can be modeled as diffuse rather than specular. Calculation of the irradiance at a location resulting from diffuse reflections depends on the total irradiance received by the reflecting source, reflectivity of the source, geometry, orientation, and distance to the source. For a diffuse source, we assume that the reflected diffuse radiance, L_d (W/m^2-sr), is uniform in all directions. The diffuse irradiance, E_d (W/m^2), received by an observer at a radial distance, r (m), from the source can be written as a function of the diffuse radiance as follows:

[2]The effective spot size assumes that the reflected sun image is circular. In reality, the shape of the reflected sun image as viewed by an observer will become elongated along the linear (long) axis of the collector with increasing distance.

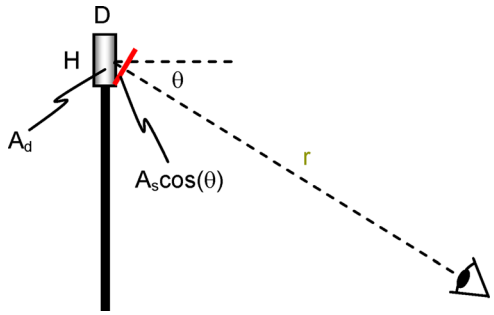

Fig. 6 Illustration of parameters used for diffuse-reflection calculations (e.g., viewing an external cylindrical receiver on top of a tower)

$$E_d = L_d \Omega \frac{A_s \cos(\theta)}{A_p} \tag{17}$$

where A_p is the pupil area (m^2), Ω is the solid angle (sr) subtended by the pupil of the eye as viewed from the source, A_s is the area of the source visible to the observer (m^2), and θ is the angle between the surface normal of the source and the line of sight between the source and the observer. The product of $A_s\cos(\theta)$ is the visible area projected toward the viewer (see Fig. 6) and is the area upon which the radiance, L_d, is based. Note that as θ increases to 90 deg, the visible source area and, hence, the diffuse irradiance goes to zero. Also, it should be noted that the visible source area, A_s, is not necessarily the same as the total area of the diffuse source, A_d. If the radiating source is planar then $A_d = A_s$. The potential for different areas of the diffuse source arise when a nonplanar source exists, such as a cylindrical external receiver. In this case, the diffuse source area, A_d, is equal to π^*D^*H, while the visible area, A_s, is approximately equal to D^*H, where D is the diameter of the cylinder and H is the height. The projected area perpendicular to the line of sight is equal to $A_s\cos(\theta)$. See Fig. 6 for a graphical representation of these parameters.

In Eq. (17), the solid angle, Ω, subtended by the pupil area, A_p, as viewed from the diffuse source, can be expressed as follows:

$$\Omega = \frac{A_p}{r^2} \tag{18}$$

An expression for the radiance, L_d, in Eq. (17) can be derived by expressing the total reflected radiative flux, E_s (W/m^2), emitted into a hemisphere from an element of the diffuse source as a function of the radiance [15],

$$E_s = \int_0^{2\pi} \int_0^{\pi/2} L_d \cos\theta \sin\theta d\theta d\phi = \pi L_d \tag{19}$$

where θ and ϕ are the polar and azimuthal angles within a hemisphere over the emitting element. Assuming the reflection is uniform over all elements comprising the diffuse source, the total hemispherical radiative flux from a single element is also equal to the total reflected power emitted from the diffuse source, P_d (W), divided by the total surface area of the diffuse source, A_d (m^2),

$$E_s = \frac{P_d}{A_d} \tag{20}$$

Combining Eqs. (17)–(20) yields the following expression for the diffuse irradiance received at a distance, r, from the diffusely reflecting source,

$$E_d = \frac{P_d}{\pi A_d} \frac{A_s \cos(\theta)}{r^2} \tag{21}$$

where the total power emitted from the diffuse source, P_d, can be expressed as the product of the direct normal irradiance, diffuse source area, reflectivity of the diffuse source, and concentration ratio of the heliostat field to the diffuse source area,

$$P_d = E_{\mathrm{DNI}} A_d \rho_d C \tag{22}$$

Combining Eq. (21) with Eqs. (1) and (2) yields the following expressions for the subtended angle, ω (rad), and diffuse retinal irradiance, $E_{r,d}$ (W/m^2), where the corneal irradiance, E_c, is set equal to the diffuse irradiance, E_d, and the source size, d_s, is determined using Eq. (12) with $A_h = A_s\cos(\theta)$,

$$\omega = \frac{\sqrt{4A_s \cos(\theta)/\pi}}{r} \tag{23}$$

$$E_{r,d} = \frac{P_d d_p^2 \tau}{4 A_d f^2} \tag{24}$$

As an example, the irradiance from a diffusely reflecting power-tower external cylindrical receiver is calculated using the following parameters:

- irradiance on power-tower receiver $= 1 \times 10^6$ W/m^2 (1000 suns at a DNI $= 1000$ W/m^2)
- radius of receiver $= 10$ m
- height of receiver $= 20$ m
- height of tower $= 100$ m
- receiver surface area $= 1257$ m^2 (calculated from receiver radius and height)
- reflectivity of receiver $= 0.1 - 0.5$.

Figure 7 shows a plot of the calculated corneal irradiance (at the front of the eye) as a function of distance from the receiver for reflectivity values of 0.1 and 0.5, assuming a diffuse radiance [Eq. (21)]. The irradiance decreases rapidly with increasing distance because the area over which the radiative power is distributed grows as a function of distance squared. Near the base of the tower at a radial distance close to 100 m (looking up at the receiver), the irradiance drops off to zero because the visible source area [modified by $\cos(\theta)$ in Eq. (21)] goes to zero.

The calculated irradiance can then be used to calculate the retinal irradiance using Eqs. (1) and (2) for comparison against the safety metrics in Fig. 2. For example, at a radial distance of 300 m (horizontal distance of 283 m), the irradiance from Eq. (21) is 0.067 W/cm^2 at a reflectivity of 0.5. The visible area, A_s, of the receiver is $20\text{ m} \times 20\text{ m} = 400\text{ m}^2$, and $\cos(\theta) = 283/300 = 0.94$. So, the projected area perpendicular to the line of sight is $400 \times 0.94 = 376\text{ m}^2$, and the effective diameter of an equivalent circular area is given by Eq. (12) as 21.9 m. The subtended angle of the receiver is then calculated as 21.9 m/300 m = 0.073 rad, and the retinal image size is 1.24×10^{-3} m using $f = 0.017$ m.

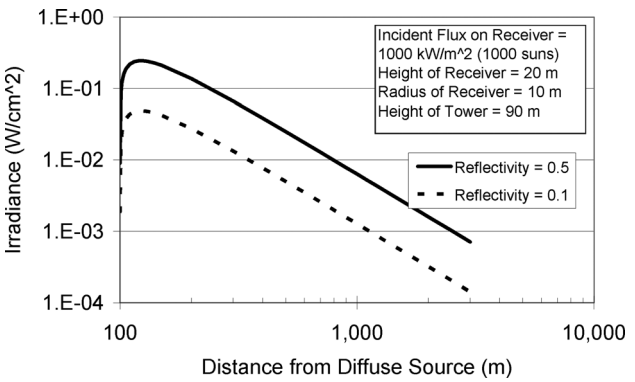

Fig. 7 Irradiance at the cornea as a function of distance from a diffuse source with different reflectivities

Equation (2) then yields a retinal irradiance of 0.087 W/cm^2 using $d_p = 0.002$ m [Eq. (24) yields the same value]. According to Fig. 2 (retinal irradiance = 0.087 W/cm^2 and subtended angle = 73 mrad), this irradiance will not cause irreversible eye damage, but it is sufficient to produce a temporary after-image if one looks directly at the source. The minimal safe distance to prevent a temporary after-image effect can be calculated by using Eqs. (5) and (23) to determine at what distance, r, the retinal irradiance (0.087 W/cm^2) is less than the after-image threshold given in Eq. (5). This distance is calculated to be approximately 1840 m, assuming no atmospheric attenuation. This large distance is a result of the large receiver size and the large amount of incident power on the receiver (1000 suns).

4 Testing and Model Validation

The specular and diffuse reflection models were evaluated via testing at the NSTTF at Sandia National Laboratories. Irradiances from specular reflections were evaluated by aiming a parabolic dish collector off-axis from the sun. Irradiances from diffuse reflections were evaluated from heliostat-generated beam images on the front wall of the central receiver tower at the NSTTF. A Nikon D70 digital single-lens reflex camera was used to capture the reflected images from the sun off both the parabolic dish and the tower wall at varying distances from the reflected image using f/32 and a shutter speed of 1/8000th second. Distances were recorded using a Bushnell Scout 1000 Rangefinder. Tiffen neutral density (ND) filters that are intended to reduce the intensity of all wavelengths of light equally, were applied to the camera lens to prevent the sunlight from saturating the image. The transmittance, T, of the ND filters is calculated as follows:

$$T = 10^{-\mathrm{OD}} \tag{25}$$

where OD is the optical density of the filter. For example, an ND0.3 filter has an optical density of 0.3 and transmits 50% of the incoming light, while an ND0.9 filter has an optical density of 0.9 and transmits only 13% of the incoming light. Direct images of the sun, which were used as a reference for the reflected images, required several filters (three ND0.9 and an ND0.3), while images of the reflections required fewer filters.

MATLAB® was used to process the raw image files by summing the pixel intensity values over the region of the reflected sun image in each photo. Each pixel value was multiplied by the filter value(s) used in each image. For example, if a single ND0.3 filter was used, the pixel value would be multiplied by 2. The sum of the pixel values for each reflected image was divided by the sum of the pixel values for the direct sun image to yield the normalized irradiance measured in suns. These values were then compared to the predicted irradiances from the models for the specular and diffuse reflection tests.

Errors associated with the predicted and measured reflected irradiance include the following: (1) uncertainty in the measured reflectivity of the glare source, (2) uncertainty in the measured distance, (3) uncertainties associated with the camera detector and ND filters, and (4) uncertainty in the area (number of pixels) associated with the reflected image (glare source). The uncertainty of the measured reflectivity can be ±2–3% for the specular surface of the dish facets, depending on the location of the measurements on the mirror versus the location of the actual reflected sun image. The uncertainty in the measured reflectivity for the diffuse tower surface was larger and is discussed later. Because the reflectivity is not used in the photographic measurements, uncertainties in the reflectivity only affect the predicted irradiance values.

The uncertainty associated with the measured distance to the reflected image is ±1 m. At distances between the observer and the glare source on the order of 10 m and 100 m, the error in the predicted irradiance is approximately 20% and 1%, respectively. The distance is not used in the photographic measurements of the irradiance.

Errors associated with camera response are expected to be small. Ulmer et al. [16] provide error estimates for camera linearity, noise (dark current, readout), and spectral influences, which can be caused by a nonconstant filter transmission as a function of radiation wavelength. Each of these factors was estimated to cause an error of approximately ±0.5% for a single pixel value. Dark current values (pixel value when no irradiance exists on the CCD) were measured to be ~0.1% of the maximum pixel value for the camera used in this study. Errors in the transmittance values associated with the ND filters can cause errors in the calculated pixel values and, hence, irradiance values. Ideally, the same ND filters should be used to record images of both the reflected and actual sun images so that any errors in the ND filter transmittance values will cancel.

The errors associated with the image processing increase with distance from the reflected image because the area representing the reflected image (i.e., number of pixels selected to represent the glare source) becomes relatively more uncertain as the image size is reduced. This can add to the uncertainty of the relative irradiance determined from the image processing algorithm. We estimate that the uncertainty in the irradiance associated with image size is less than 2–3% since the pixel values corresponding to regions outside the reflected image will be small relative to the pixel values corresponding to regions within the reflected image. To reduce these errors, one can zoom in to fill the camera screen as much as possible with the reflected or actual sun images. When determining the corneal irradiance, the zoom (camera focal length) can be different between photos of the reflected and actual sun images since the cumulative power represented by all pixels comprising the reflected and actual sun images is used (as opposed to the power received by an individual pixel). However, if the subtended angle of the glare source is desired, the zoom should be held constant so that the subtended angle of the sun can be used to determine the subtended angle of the reflected image (assuming the camera focal length is constant). The camera settings that control how much light enters the iris (f-stop and shutter speed) should also be kept constant when comparing images between the reflected and actual sun images.

4.1 Specular Reflection Tests. The specular reflection tests were conducted on July 1, 2009, at approximately 9:30 AM (mountain daylight time (MDT)) with a direct normal irradiance of approximately 850 W/m^2. The Mod 2-2 10 kW parabolic dish used in the tests had a focal length of 5.448 m, a diameter of 8.8 m, a measured reflectivity of 0.93, and an estimated rms slope error of 1 mrad [17]. An rms slope error of 1 mrad results in a total beam divergence angle, β, of 11.4 mrad [9.4 mrad (from subtended sun angle) + 0.001 mrad*2 (pointing error)]. The dish was positioned so that the reflected image of the sun was visible on mirror facets of the dish as the observer moved in a southerly direction away from the dish. Photos of the reflected image on the dish were taken at varying distances, and the images were processed in MATLAB®. Results are shown in Fig. 8, along with the analytical predictions using Eq. (11) (where E_{beam} is divided by E_{DNI} to get the normalized irradiance).

A commercial ray-tracing code, ASAP®, was also used to model this system using the parameters described above, and the results are shown in Fig. 8. In the ray-tracing simulations, up to 20×10^6 rays were used to simulate the average irradiance on a small target located at different distances from the collector, representative of the observer (camera) locations in the test. The dish was modeled as an ideal paraboloidal collector with the dimensions and optical characteristics described above. A mirror random-roughness model corresponding to an rms slope error of 1 mrad [17] was used in the ray-tracing model. Apodization of the source rays was also included to account for sun shape and limb darkening [18].

The results show that the measured and predicted normalized irradiance from the specularly reflected image of the sun on the

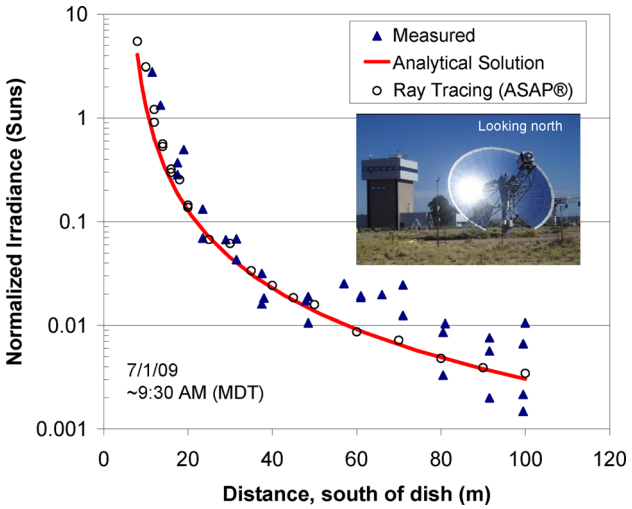

Fig. 8 Predicted and measured normalized irradiance as a function of distance caused by specular reflections from the Mod 2-2 10 kW parabolic dish

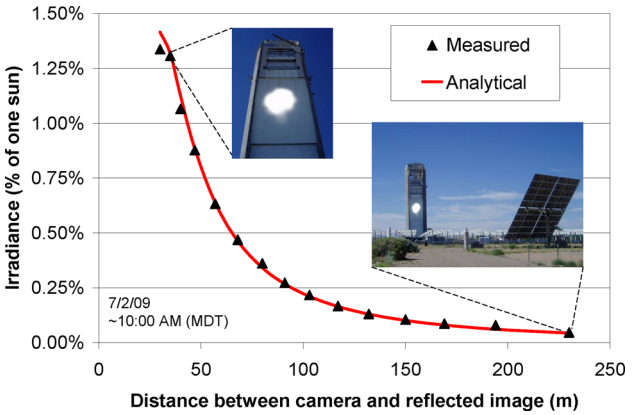

Fig. 9 Predicted and measured normalized irradiance as a function of distance caused by diffuse reflections from the NSTTF central receiver tower

dish facets match very well over the range of distances tested. At small distances (within two focal lengths), the normalized irradiance can exceed 1 sun. At greater distances, the normalized irradiances decrease rapidly due to the diverging beam. It is interesting to note that the analytical solution, which assumes a uniform sun intensity and neglects off-axis aberrations, matches extremely well with the ray-tracing solution, which rigorously includes these effects. This demonstrates that the analytical solution can be used to give good estimates of the average irradiance as a function of distance from the specular reflection, even with off-axis conditions.

The average irradiance, which represents the irradiance at the cornea at a particular distance, can then be used to determine the retinal irradiance for comparison against the safety metrics. For example, at a distance of 40 m, the normalized irradiance is approximately 0.02 suns. From Eq. (13), the subtended angle formed by the reflected image of the sun on the dish is calculated as 1.7 mrad, where $E_{\text{beam}}/E_{\text{DNI}}$ is the normalized irradiance of 0.02 suns, $\rho = 0.93$ and $\beta = 11.4$ mrad. Assuming a direct normal irradiance of 0.1 W/cm^2 (equal to one sun), the retinal irradiance is then calculated to be ~ 5 W/cm^2 using Eqs. (1) and (2) with $d_p = 0.002$ m, $f = 0.017$ m, and $\tau = 0.5$. According to Fig. 2, a retinal irradiance of 5 W/cm^2 with a subtended angle of 1.7 mrad is less than the safe retinal irradiance metrics to prevent permanent eye damage. However, the calculated irradiance is sufficient to potentially cause a temporary after-image if one were to view directly at the reflected image. Equations (5), (11), and (13) yield a minimal distance of 55 m for this system to yield a low potential for after-image effects.

4.2 Diffuse Reflection Tests. The diffuse reflection tests were conducted on July 2, 2009, at approximately 10:00 AM (MDT) with a direct normal irradiance of approximately 880 W/m^2. A 147 m^2 ATS heliostat with a reflectivity of ~ 0.9 was used to concentrate a beam of sunlight onto the front of the NSTTF central receiver tower that was painted white. The reflection of the sunlight from the front of the painted tower was approximately diffuse based on reflectivity measurements taken later with a Surface Optics, Inc. 410 Solar reflectometer. Reflectivity measurements ranged from ~ 0.4 (in pitted and soiled regions) to ~ 0.8. In all measurements, the diffuse component of the reflectivity was $>99\%$ of the total reflectivity. Photos of the beam on the tower were taken at varying distances from the tower, and the images were processed in MATLAB® to determine the normalized irradiance values. Analytical predictions of the irradiance as a function of distance were made using Eq. (21), where the diffuse power emanating from the tower is calculated as the total incident power on the tower times the reflectivity of the tower. The total incident power is calculated as the product of the DNI (880 W/m^2), the surface area of the heliostat (147 m^2), the reflectivity of the heliostat (0.9), and the cosine loss (0.78) due to the off-axis position of the heliostat (calculated at the date and time of the test), which yields 91 kW. The total diffusely reflected power, P_d, emitted from the front of the tower is equal to the incident power times the reflectivity of the white paint on the tower.

Figure 9 shows the results of the measured and predicted irradiances normalized to the DNI, assuming an average reflectivity of 0.7 for the white paint in the predicted values. Reflectivity measurements ranged from ~ 0.4 to ~ 0.8, with most of the measurements closer to 0.8. An average reflectivity value of 0.7 was used because it gave the best fit to the data. Results show that the measured and predicted irradiances match very closely and follow the same trend as a function of distance from the source. At close distances, both the predicted and measured irradiances show a slight decrease in the slope of the irradiance, which is caused by the reduced visible area of the reflected sun image at large viewing angles [cosine loss in Eq. (21)]. This demonstrates that the analytical solution can be used to estimate the irradiance as a function of distance from diffuse reflections.

5 Summary and Conclusions

This paper has presented methods to evaluate potential glint and glare hazards from specularly and diffusely reflected sunlight from concentrating solar collectors. First, a review of metrics was presented to determine safe retinal irradiances as a function of subtended source angle (or retinal image size). Metrics for both permanent eye damage and temporary after-image effects were included. Analytical models were then derived to calculate irradiances from both specular and diffuse sources. These models were validated using data collected from specular and diffuse reflection tests.

The methods and equations presented in this paper can be used to calculate irradiances from various concentrating solar collector systems (e.g., heliostats, dishes, troughs, receivers). The calculated retinal irradiance can be compared against the safe retinal irradiance metrics to evaluate potential glint and glare hazards. It should be noted, however, that the quantified metrics and estimates for retinal irradiance do not account for all factors. For example, atmospheric attenuation and the impact of wearing sunglasses are not considered in the models. In addition, human

factors and behaviors are not assessed in this paper, which may affect the impact of different glint and glare scenarios.

The impact of multiple coincident beams (i.e., from adjacent collectors or receivers) was not considered in this study. Brumleve (pp. 27–32) [1] provides a discussion of the impact of multiple sources that can be used together with the results of this study. In general, multiple sources can increase the retinal image size. In addition, the retinal irradiance may or may not increase depending on whether the projected retinal images overlap, which depends on the positions of the sources relative to the observer. For example, if two beams enter the eye but do not overlap, the affected retinal image area is increased, but the irradiance (W/cm^2) is the same as that from a single beam. If the two beams are nearly coincident and form a coalesced image on the retina, the retinal image size is about the same but the irradiance increases.

Based on the configurations and operation of the various concentrating solar technologies, potential glint and glare scenarios that should be considered include the following:

- Power-towers
  - Specular reflections from heliostats when they are moving to or from stowed position, in standby mode, or not aimed at the receiver.
  - Diffuse reflections from the receiver.
- Linear collectors
  - Specular reflections from the mirrors when they are moving to or from stowed position and from specular reflections off the ends of the trough or mirrors when the sun is low and aligned with the mirrors (e.g., reflections from the north end of a north–south field when the sun is low in the southern horizon).
  - Diffuse and specular reflections from receiver tubes and bellows shields.
- Dish/engine systems
  - Specular reflections from mirror facets when the dish is off-axis (offset position) or moving to or from a stowed position.
  - Diffuse reflections from the receiver aperture.

Acknowledgment

The authors would like to thank Brian Myer, John Quintana, Kirill Trapeznikov, and Chuck Andraka for their assistance with the dish testing and MATLAB image processing. The authors also thank Siri Khalsa for his assistance compiling and interpreting the safety metrics.

Sandia National Laboratories is a multiprogram laboratory managed and operated by Sandia Corporation, a wholly owned subsidiary of Lockheed Martin Corporation, for the U.S. Department of Energy's National Nuclear Security Administration under Contract No. DE-AC04-94AL85000.

Nomenclature

A = area (m^2)
A_d = total area of diffuse source (m^2)
A_s = visible surface area (m^2)
b = focal length (m)
C = concentration ratio
d, D = diameter (m)
E = irradiance (W/m^2 or W/cm^2)
E_s = reflected radiative flux emitted from diffuse source (W/m^2)
f = eye focal length (~0.017 m)
L = radiance (W/m^2-sr)
ND = neutral density
OD = optical density of filter
P = power (W)
r = distance (m)
R_x = beam radius at distance x from the mirror (m)
R_1 = portion of beam radius caused by spreading due to subtended angle of the sun and mirror contour inaccuracies (slope error) (m)
R_2 = portion of beam radius caused by focusing and defocusing characteristics of the mirror (m)
rms = root mean square
T = transmittance
x = distance (m)

Subscripts

beam = specular beam of sunlight
burn = retinal burn threshold
c = cornea
d = diffuse
DNI = direct normal irradiance
flash = after-image or flash blindness threshold
flat = flat mirror
h = heliostat
p = pupil
r = retinal
s = source
spot = reflected sun image on mirror
x = distance (m)

Greek Symbols

β = beam divergence angle (rad)
φ = azimuthal angle in hemisphere (rad)
ρ = reflectivity
θ = angle between surface normal of the source and line of sight between the source and the observer; also the polar angle in a hemisphere (rad)
τ = ocular transmission coefficient (~0.5)
ω = subtended angle (rad)
Ω = Subtended solid angle (sr)

References

[1] Brumleve, T. D., 1977, "Eye Hazard and Glint Evaluation for the 5-MWt Solar Thermal Test Facility," Sandia National Laboratories, Report No. SAND76-8022.
[2] Brumleve, T. D., 1984, "10 MWe Solar Thermal Central Receiver Pilot Plant: Beam Safety Tests and Analyses," Sandia National Laboratories, Report No. SAND83-8035.
[3] Sliney, D. H., and Freasier, B. C., 1973, "Evaluation of Optical Radiation Hazards," Appl. Opt., **12**(1), pp. 1–24.
[4] Carrier, J., 2008, "Beam Safety Design Parameters," Data Response Attachment DR89-1, Appendix A, Data Response Set 1A. Dated on Jan. 14, 2008, CH2MHILL, Ivanpah Solar Electric Generating System, Application for Certification (07-AFC-5), Submitted to California Energy Commission, http://www.energy.ca.gov/sitingcases/ivanpah/documents/applicant/DR_1a/2008-01-14_ISEGS_DR_SET_1A.PDF
[5] Carrizo Energy, LLC, 2008, "Responses to CEC Data Requests (#1–78)," Application for Certification (07-AFC-8), Carrizo Energy Solar Farm, Submitted to California Energy Commission, http://www.energy.ca.gov/sitingcases/carrizo/documents/applicant/2008-02-27_DATA_RESPONSES_1-78.PDF
[6] City of Victorville, 2008, "Victorville 2 Hybrid Power Project," Application for Certification (07-AFC-1), submitted to California Energy Commission, www.energy.ca.gov/sitingcases/victorville2/documents/
[7] San Joaquin Solar 1, 2 – Application for Certification Volume 2, Appendix L, "Glint and Glare Study," http://www.energy.ca.gov/sitingcases/sjsolar/documents/applicant/afc/AFC_volume_02/
[8] SES Solar Two, LLC (2008), "SES Solar Two Project," Application for Certification (08-AFC-5), submitted to California Energy Commission.
[9] Ho, C. K., Ghanbari, C. M., and Diver, R. B., 2009, "Hazard Analyses of Glint and Glare From Concentrating Solar Power Plants," in *Proceedings of SolarPACES 2009*, Berlin, Germany, Sept. 15–18, Report No. SAND2009-4131C.
[10] Sliney, D. H., 1980, "An Evaluation of the Potential Hazards of the Point Focusing Solar Concentrators at the JPL-Edwards Test Site," Report submitted to the Jet Propulsion Laboratory (JPL Consulting Agreement No. JF 714696), California Institute of Technology.
[11] Delori, F. C., Webb, R. H., and Sliney, D. H., 2007, "Maximum Permissible Exposures for Ocular Safety (ANSI 2000), With Emphasis on Ophthalmic Devices," J. Opt. Soc. Am. A, **24**(5), pp. 1250–1265.

[12] Metcalf, R. D., and Horn, R. E., 1958, "Visual Recovery Times From High-Intensity Flashes of Light," Air Force Aerospace Medical Research Lab, Wright Air Development Center, Technical Report No. 58232.
[13] Severin, S. L., Newton, N. L., and Culver, J. F., 1962, "An Experimental Approach to Flash Blindness," Aerosp. Med., **33**(10), pp. 1199–1205.
[14] Saur, R. L., and Dobrash, S. M., 1969, "Duration of Afterimage Disability After Viewing Simulated Sun Reflections," Appl. Opt., **8**(9), pp. 1799–1801.
[15] Incropera, F. P., and DeWitt, D. P., 1985, *Introduction to Heat Transfer*, Wiley, New York, pp. 514–515.
[16] Ulmer, S., Reinalter, W., Heller, P., Lupfert, E., and Martinez, D., 2002, "Beam Characterization and Improvement With a Flux Mapping System for Dish Concentrators," ASME J. Sol. Energy Eng., **124**, pp. 182–188.
[17] Diver, R. B., Andraka, C. E., Rawlinson, K. S., Moss, T. A., Goldberg, V., and Thomas, G., 2003, "Status of the Advanced Dish Development System Project," *Proceedings of ISEC 2003, 2003 ASME International Solar Energy Conference*, Hawaii, Mar. 15–18.
[18] Rabl, A., and Bendt, P., 1982, "Effect of Circumsolar Radiation on Performance of Focusing Collectors, ASME J. Sol. Energy Eng., **104**, pp. 237–250.